Inorg. Chem. **2008**, *47*, 11180−11190

Synthesis, Magnetism, and High-Frequency EPR Spectroscopy of a Family of Mixed-Valent Cuboctahedral Mn_{13} Complexes with 1,8-Naphthalenedicarboxylate Ligands

Christos Lampropoulos,[†] Changhyun Koo,[‡] Stephen O. Hill,[‡] Khalil Abboud,[†] and George Christou*[,†]

Departments of Chemistry and Physics, University of Florida, Gainesville, Florida 32611

Received August 5, 2008

Four mixed-valent ($Mn^{IV}Mn^{III}_6Mn^{II}_6$) tridecanuclear Mn clusters $[Mn_{13}O_8(OH)_6(ndc)_6]$ (**1**), $[Mn_{13}O_8(OEt)_5(OH)(ndc)_6]$ (**2**), $[Mn_{13}O_8(O_2CPh)_{12}(OEt)_6]$ (**3**), and $[Mn_{13}O_8(OMe)_6(ndc)_6]$ (**4**) are reported, where $ndcH_2$ is 1,8-naphthalenedicarboxylic acid. This is the first use of the latter in Mn chemistry. Complexes **1**−**3** are essentially isostructural and possess a central core composed of three layers. The middle layer consists of a Mn^{II}_6 hexagon containing a central Mn^{IV} atom, and above and below this are Mn^{III}_3 triangular units. These core Mn atoms are held together by a combination of O^{2-}, RO^-, or HO^- bridging groups. The overall metal topology is an unusual one, with the overall geometry being a metal-centered cuboctahedron (heptaparallelohedron). Variable-temperature, solid-state dc, and ac magnetization studies were carried out on complexes **1**−**4** in the 5.0−300 K range. Compound **1** was found to possess an $S = 9/2$ ground-state spin, whereas **2**, **3**, and **4** have an $S = 11/2$ ground state. Fitting of the magnetization (M) versus field (H) and temperature (T) data by matrix diagonalization and including only axial zero-field splitting, D, gave $D = -0.14$ cm^{-1} for **1**. High-frequency EPR studies were carried out on single crystals of **1**·*x*DMF, and these confirmed D to be very small, that is, **1** is essentially isotropic. The combined work demonstrates the ligating ability of 1,8-naphthalenedicarboxylate, notwithstanding its robust organic backbone and the restricted parallel disposition of its two carboxylate moieties, and its usefulness in the synthesis of new polynuclear Mn_x clusters. The work also demonstrates a sensitivity of the ground-state spin in this Mn_{13} family of complexes to relatively small structural perturbations, while the high-frequency EPR study demonstrated the magnetically isotropic nature of the Mn_{13} core.

Introduction

The synthesis and study of large assemblies of paramagnetic 3d transition metal ions has been a well-established research area for a long time. Nevertheless, it has been greatly stimulated by being the main source of single-molecule magnets (SMMs). These are molecules, usually of manganese, that can function as molecular superparamagnets and thus below their blocking temperature (T_B) can function as nanoscale magnets. SMMs combine a large ground-state spin (S) with a relatively large easy-axis magnetoanisotropy, corresponding to a negative zero-field splitting parameter, D. As a result, SMMs exhibit magnetization hysteresis in magnetization versus applied field studies, the classical, diagnostic property of a magnet.[1] Manganese clusters have been the main source of SMMs primarily because they often

* To whom correspondence should be addressed. Tel.: +1-352-392-8314. Fax: +1-352-392-8757. E-mail: christou@chem.ufl.edu.
[†] Department of Chemistry.
[‡] Department of Physics.

(1) (a) Christou, G.; Gatteschi, D.; Hendrickson, D. N.; Sessoli, R. *MRS Bulletin* **2000**, *25*, 66. (b) Sessoli, R.; Tsai, H.-L.; Schake, A. R.; Wang, S.; Vincent, J. B.; Folting, K.; Gatteschi, D.; Christou, G.; Hendrickson, D. N. *J. Am. Chem. Soc.* **1993**, *115*, 1804. (c) Sessoli, R.; Gatteschi, D.; Caneschi, A.; Novak, M. A. *Nature* **1993**, *365*, 141. (d) Christou, G. *Polyhedron* **2005**, *24*, 2065. (e) Wernsdorfer, W.; Aliaga-Alcalde, N.; Hendrickson, D. N.; Christou, G. *Nature* **2002**, *416*, 406. (f) Soler, M.; Wernsdorfer, W.; Abboud, K. A.; Hendrickson, D. N.; Christou, G. *Polyhedron* **2003**, *22*, 1777. (g) Soler, M.; Wernsdorfer, W.; Abboud, K. A.; Huffman, J. C.; Davidson, E. R.; Hendrickson, D. N.; Christou, G. *J. Am. Chem. Soc.* **2003**, *125*, 3576. (h) Andres, H.; Basler, R.; Blake, A. J.; Cadiou, C.; Chaboussant, G.; Grant, C. M.; Güdel, H.-U.; Murrie, M.; Parsons, S.; Paulsen, C.; Semadini, F.; Villar, V.; Wernsdorfer, W.; Winpenny, R. E. P. *Chem.—Eur. J.* **2002**, *8*, 4867. (i) Brechin, E. K.; Soler, M.; Christou, G.; Helliwell, M.; Teat, S. J.; Wernsdorfer, W. *Chem. Commun.* **2003**, 1276. (j) Price, D. J.; Batten, S. R.; Moubaraki, B.; Murray, K. S. *Chem. Commun.* **2002**, 762.

10.1021/ic801484g CCC: $40.75
Published on Web 10/25/2008

display unusually large ground state S values, and reasonably large D values arising from the presence of Jahn−Teller distorted Mn^{III} ions; the barrier to magnetization reversal has a maximum value given by $S^2|D|$ and $(S^2 - 1/4)|D|$ for integer and half-integer spins, respectively. In addition, SMMs are small enough that they truly straddle the classical/quantum interface, displaying not just the classical property of magnetization hysteresis but also the quantum properties of quantum tunneling of the magnetization (QTM)[2] and quantum phase interference.[3]

The rational synthesis of Mn clusters has been a challenge to groups worldwide. Our own group has previously reported Mn SMMs with metal nuclearities ranging from Mn_3[4] to Mn_{84}.[5] To date, the most well studied SMMs are the $[Mn_{12}O_{12}(O_2CR)_{16}(H_2O)_4]^{z-}$ (R = various; $z = 0-3$) family containing monocarboxylate groups. Indeed, monocarboxylic acids have been the primary ligand type in high-spin clusters to date. In contrast, polynuclear 3d metal clusters containing dicarboxylate groups are much less common in the inorganic literature. Our own group has reported only a few Mn clusters containing dicarboxylates,[6,7] and we recently decided to extend these investigations. The idea is that the restricted flexibility of two linked carboxylate groups may yield products that are different from those with monocarboxylate groups. This was certainly the case in our previous work with phthalic acid[6a] and 2,2′-diethylmalonic acid.[7] For the present work, we decided to explore a dicarboxylic acid with an even more restricted flexibility and chose 1,8-naphthalenedicarboxylic acid ($ndcH_2$), in which the two carboxylate groups are very close and parallel to each other on a rigid naphthalene backbone. We were unaware of any previous reports of crystallographically characterized products from the use of $ndcH_2$ in Mn chemistry.

We herein report that the reactions of ($ndcH_2$) with common Mn starting materials have led to the formation of new Mn_{13} clusters. These contain Mn atoms in three oxidation states (II, III, and IV). We were also subsequently able to isolate a complex with the same core using only the monocarboxylate ligand benzoate, showing that the dicarboxylate is not strictly speaking essential for forming the Mn_{13} cluster, although it does yield more robust products. Nevertheless, the benzoate complex has allowed a comparative study of the structures and magnetic properties of this family of related Mn_{13} complexes. Portions of this work have been previously communicated.[8]

Experimental Section

Syntheses. All manipulations were performed under aerobic conditions using chemicals as received, unless otherwise stated. $[Mn_3O(O_2CPh)_6(py)_2(H_2O)]$ was prepared as previously reported.[9]

$[Mn_{13}O_8(OH)_6(ndc)_6]$ (1). To a stirred solution of $Mn(O_2CMe)_2\cdot 4H_2O$ (0.20 g, 0.8 mmol) in DMF (15 mL) was added dropwise a suspension of 1,8-naphthalic acid anhydride (0.20 g, 1.0 mmol) and NEt_3 (1.40 mL, 10 mmol) in DMF (15 mL), resulting in a dark brown solution. This was stirred for a further 2 h and filtered, and the filtrate was layered with an equal volume of Et_2O. The solution was left undisturbed at ambient temperature for 2 days, during which time large brown crystals of **1**·xDMF grew; the yield was ∼70%. The crystals were maintained in mother liquor for X-ray crystallography and other single-crystal studies or collected by filtration, washed with Et_2O, and dried in vacuo. Anal. Calcd (Found) for **1**·8DMF·H_2O: C, 40.71 (40.99); H, 3.56 (3.44); N, 3.96 (3.98) %. Selected IR data (KBr disk, cm^{-1}): 3391(w), 2923(m), 2360(m), 1652(s), 1557(s), 1420(s), 1350(s), 1225(m), 1100(m), 843(m), 811(m), 718(s), 610(m), 600(w), 526(s).

$[Mn_{13}O_8(OEt)_5(OH)(ndc)_6]$ (2). To a stirred solution of $Mn(O_2CMe)_2\cdot 4H_2O$ (0.20 g, 0.8 mmol) in MeCN (20 mL) was added dropwise a suspension of 1,8-naphthalic anhydride (0.20 g, 1.0 mmol) and NEt_3 (1.40 mL, 10 mmol) in EtOH (10 mL), resulting in a dark brown solution. The solution was stirred for a further 2 h and filtered, and the filtrate was layered with EtOH. The solution was left undisturbed at ambient temperature for 2 days, during which time large brown crystals of **2**·xMeCN formed; the yield was ∼65%. The crystals were maintained in mother liquor for X-ray crystallography and other single-crystal studies or collected by filtration, washed with cold EtOH, and dried in air. Anal. Calcd (Found) for **2**·6MeCN: C, 42.29 (42.54); H, 3.25 (3.74); N, 3.15 (2.79) %. Selected IR data (KBr, cm^{-1}): 3397(w), 2354(m), 1558(s), 1420(s), 1351(s), 1225(m), 1029(m), 873(m), 839(m), 811(m), 780(s), 613(m), 600(w), 527(s).

$[Mn_{13}O_8(OEt)_6(O_2CPh)_{12}]$ (3). To a stirred solution of $[Mn_3O(O_2CPh)_6(py)_2(H_2O)]$ (0.50 g, 0.5 mmol) in a 1:3 (v/v) mixture of MeCN/EtOH (30 mL) was added NEt_3 (0.50 mL, 3.5 mmol) in small portions, resulting in a dark brown solution. The solution was stirred for a further 20 min and filtered, and the filtrate was layered with Et_2O. The solution was left undisturbed at ambient temperature for 2 days, during which time large brown crystals of **3**·4MeCN grew; the yield was ∼80%. The crystals were maintained in mother liquor for X-ray crystallography and other single-crystal studies or collected by filtration, washed with Et_2O, and dried in vacuo. Dried solid appears to be hygroscopic and analyzed as **3**·$7H_2O$. Anal. Calcd (Found) for **3**·$7H_2O$: C, 42.54 (42.83); H, 3.48 (3.89); N, 0.12 (0.00) %. Selected IR data (KBr, cm^{-1}): 3397(w), 3059(m), 2969(m), 2923(m), 2878(m), 1597(s), 1553(s), 1410(s), 1402(w), 1379(s), 1176(m), 1027(s), 873(m), 712(s), 685(s), 639(s), 585(s), 560(w), 549(s), 477(s).

$[Mn_{13}O_8(OMe)_6(ndc)_6]$ (4). To a stirred solution of $Mn(O_2CMe)_2\cdot 4H_2O$ (0.20 g, 0.8 mmol) in DMF (15 mL) was added dropwise a suspension of 1,8-naphthalic acid anhydride (0.2 g, 1 mmol) and NEt_3 (1.4 mL, 10 mmol) in DMF (15 mL), resulting in a dark brown solution. This was stirred for a further 2 h, filtered, and layered

(2) Friedman, J. R.; Sarachik, M. P. *Phys. Rev. Lett.* **1996**, *76*, 3830.
(3) (a) Wernsdorfer, W.; Sessoli, R. *Science* **2000**, 2417. (b) Wernsdorfer, W.; Soler, M.; Christou, G.; Hendrickson, D. N. *J. Appl. Phys.* **2002**, *91*, 7164. (c) Wernsdorfer, W.; Chakov, N. E.; Christou, G. *Phys. Rev. Lett.* **2005**, *95*, 1–4.
(4) (a) Stamatatos, T. C.; Foguet-Albiol, D.; Stoumpos, C. C.; Raptopoulou, C. P.; Terzis, A.; Wernsdorfer, W.; Perlepes, S. P.; Christou, G. *J. Am. Chem. Soc.* **2005**, *127*, 15380. (b) Stamatatos, T. C.; Foguet-Albiol, D.; Lee, S.-C.; Stoumpos, C. C.; Raptopoulou, C. P.; Terzis, A.; Wernsdorfer, W.; Hill, S. O.; Perlepes, S. P.; Christou, G. *J. Am. Chem. Soc.* **2007**, *129*, 9484–9499.
(5) Tasiopoulos, A. J.; Vinslava, A.; Wernsdorfer, W.; Abboud, K. A.; Christou, G. *Angew. Chem., Int. Ed.* **2004**, *43*, 2117.
(6) (a) Squire, R. C.; Aubin, S. M. J.; Folting, K.; Streib, W. E.; Christou, G.; Hendrickson, D. N. *Inorg. Chem.* **1995**, *34*, 6463. (b) Canada-Vilalta, C.; Streib, W. E.; Huffman, J. C.; O'Brien, T. A.; Davidson, E. R.; Christou, G. *Inorg. Chem.* **2004**, *43*, 101.
(7) Wemple, M. W.; Tsai, H. L.; Wang, S.; Claude, J. P.; Streib, W. E.; Huffman, J. C.; Hendrickson, D. N.; Christou, G. *Inorg. Chem.* **1996**, *35*, 6437.
(8) Lampropoulos, C.; Murugesu, M.; Abboud, K. A.; Christou, G. *Polyhedron* **2007**, *26*, 2129.
(9) Vincent, J. B.; Chang, H. R.; Folting, K.; Huffman, J. C.; Christou, G.; Hendrickson, D. N. *J. Am. Chem. Soc.* **1987**, *109*, 5703.

Table 1. Crystal Data and Structure Refinement Parameters for Complexes **1**−**3**

parameter	**1**·*x*DMF	**2**·*x*MeCN	**3**·4MeCN
formula[a]	$C_{330}H_{360}Mn_{39}N_{38}O_{152}$	$C_{91}H_{80}Mn_{13}N_4O_{39}$	$C_{104}H_{102}Mn_{13}N_4O_{38}$
fw, g/mol[a]	9433.22	2567.81	2730.12
space group	$P\bar{1}$	$P\bar{1}$	$C2/c$
a, Å	17.1761(10)	15.0588(2)	25.580(3)
b, Å	22.9617(14)	15.2249(2)	15.1050(15)
c, Å	24.9168(15)	15.3862(2)	28.771(3)
α, deg	74.456(1)	112.591(2)	90
β, deg	85.032(1)	118.922(2)	100.315(2)
γ, deg	86.978(1)	94.82(2)	90
V, Å^3	9427.5(10)	2687.1(3)	10937(2)
Z	1	1	4
T, K	173(2)	173(2)	173(2)
radiation, Å[b]	0.71073	0.71073	0.71073
ρ_{calcd}, mg/m^3	1.662	1.587	1.658
μ, mm^{-1}	1.352	1.552	1.530
R1[c,d]	0.0628	0.0632	0.0490
wR2[e]	0.1718	0.1830	0.1019

[a] Including solvate molecules. [b] Graphite monochromator. [c] $I > 2\sigma(I)$. [d] $R1 = 100\Sigma(||F_o| - |F_c||/\Sigma|F_o|$. [e] $wR2 = 100[\Sigma[w(F_o^2 - F_c^2)^2]/\Sigma[w(F_o^2)^2]]^{1/2}$, $w = 1/[\sigma^2(F_o^2) + [(ap)^2 + bp]$, where $p = [\max(F_o^2, O) + 2F_c^2]/3$.

with an equal volume of MeOH. The solution was left undisturbed at ambient temperature for 2 days, during which time large brown crystals formed; the yield was ∼68%. The crystals were collected by filtration, washed with cold MeOH and Et_2O, and dried in vacuo. Anal. Calcd (Found) for **4**·5DMF·H_2O: C, 41.42 (41.27); H, 3.40 (3.40); N, 2.60 (2.94) %. Selected IR data (KBr, cm-1): 3419(w), 2361(m), 2336(m), 1653(s), 1558(s), 1415(s), 1351(s), 1225(m), 1018(m), 843(m), 814(m), 781(s), 645(w), 600(w), 525(s).

X-ray Crystallography. All data were collected at 173 K on a Siemens SMART PLATFORM equipped with a CCD area detector and a graphite monochromator utilizing Mo Kα radiation (λ = 0.71073 Å). Cell parameters were refined using up to 8192 reflections. A full sphere of data (1850 frames) was collected using the ω-scan method (0.3° frame width). The first 50 frames were remeasured at the end of data collection to monitor instrument and crystal stability (maximum correction on I was < 1%). Absorption corrections by integration were applied based on measured indexed crystal faces. The structures were solved by direct methods in *SHELXTL6* and refined on F^2 using full-matrix least-squares. The non-H atoms were treated anisotropically, whereas the H atoms were placed in ideal positions and refined as riding on their C atoms. Data collection parameters and structure solution details are listed in Table 1.

For **1**·*x*DMF, the asymmetric unit consists of three half-clusters and ∼19 DMF molecules. The latter were disordered and could not be modeled properly, thus program SQUEEZE, a part of the PLATON package of crystallographic software, was used to calculate the total solvent area and remove its contribution to the overall intensity data. Each half-cluster has four bridging OH^- groups whose H atoms were located in difference Fourier maps but did not refine properly. Thus they were included in the final refinement cycle in idealized positions and refined riding on their parent atoms. A total of 1666 parameters were refined in the final cycle of refinement using 41 405 reflections with $I > 2\sigma(I)$ to yield R1 and wR2 of 6.28% and 14.94%, respectively.

For **2**·*x*MeCN, the asymmetric unit consists of a half-cluster and some MeCN molecules. The latter were disordered and could not be modeled properly, thus program SQUEEZE was used to calculate the solvent disorder area and remove its contribution to the overall intensity data. The cluster has one EtO^- ligand (O17) with its methyl group disordered, and this was refined in two positions with the site occupation factors dependently refined. Another disorder is located on another EtO^- ligand (O19), which is disordered with a OH^- group with occupancies of 50/50; the half-occupancy OH^- component is H-bonded to a (half-occupancy) EtOH group. The compound formula is thus $[Mn_{13}O_8(OEt)_5(OH)(ndc)_6]$. A total of 598 parameters were refined in the final cycle of refinement using 15 010 reflections with $I > 2\sigma(I)$ to yield R1 and wR2 of 6.32% and 16.89%, respectively.

For **3**·4MeCN, the asymmetric unit consists of a half-cluster and two MeCN molecules. The latter were each disordered about two sites, and they were refined with each site occupation factor fixed at 0.5. A total of 712 parameters were refined in the final cycle of refinement using 9104 reflections with $I > 2\sigma(I)$ to yield R1 and wR2 of 4.90% and 7.35%, respectively.

Other Studies. Infrared spectra were recorded in the solid state (KBr pellets) on a Nicolet Nexus 670 FTIR spectrometer in the 400−4000 cm^{-1} range. Elemental analyses (C, H, and N) were performed by the in-house facilities of the University of Florida Chemistry Department. Variable-temperature dc and ac magnetic susceptibility data were collected at the University of Florida using a Quantum Design MPMS-XL SQUID susceptometer equipped with a 7 T magnet and operating in the 1.8−300 K range. Samples were embedded in solid eicosane to prevent torquing. Magnetization versus field and temperature data were fit using the program MAGNET.[10] Pascal's constants were used to estimate the diamagnetic correction, which was subtracted from the experimental susceptibility to give the molar paramagnetic susceptibility (χ_M). High-frequency (40−160 GHz) electron paramagnetic resonance (HFEPR) measurements were carried out using a millimeter-wave vector network analyzer (MVNA) in combination with a cavity perturbation technique described elsewhere.[11] Magnetic fields up to 17 T were provided by an axial superconducting magnet, and angle-dependent HFEPR data were obtained using a cavity that allowed rotation of the sample about one axis perpendicular to the applied field.[12] The temperature was controlled via a variable-flow cryostat situated within the bore of the magnet, using a calibrated Cernox resistor as a reference.

Results and Discussion

Syntheses. The most commercially convenient source of 1,8-naphthalenedicarboxylic acid is the anhydride 1,8-naphthalic anhydride, and so we employed this in the presence of base to foster in situ formation of the dicarboxylate ndc^{2-}. For completeness, we also prepared and recrystallized the diacid form $ndcH_2$, using the published procedure that starts with the anhydride,[13] and investigated its use in place of the anhydride in the described reactions. The preformed dicarboxylic acid offers some advantages in being more soluble than the anhydride, but we found that it gives the same products in similar (or lower) yields as the more convenient reactions starting with the anhydride, and so we document only the latter in the Experimental Section. The low solubility of the anhydride was overcome by using DMF and MeCN/EtOH reaction solvents for the syntheses of **1** and **2**, respectively.

We originally obtained $[Mn_{13}O_8(OH)_6(ndc)_6]$ (**1**) from the reaction of $[Mn_{12}O_{12}(O_2CMe)_{16}(H_2O)_4]$[14] with eight equiva-

(10) Davidson, E. R. *MAGNET*; Indiana University: Bloomington, IN, 1999.
(11) Mola, M.; Hill, S.; Goy, P.; Gross, M. *Rev. Sci. Instrum.* **2000**, *71*, 186.
(12) Takahashi, S.; Hill, S. *Rev. Sci. Instrum.* **2005**, *76*, 023114.
(13) Fitzgerald, L. J.; Gallucci, J. C.; Gerkin, R. E. *Acta Crystallogr.* **1991**, *B47*, 776.
(14) Lis, T. *Acta Crystallogr.* **1980**, *B36*, 2042.

lents of the preformed 1,8-naphthalene dicarboxylic acid, but we subsequently derived the superior procedure described. This involves reaction of Mn^{II} with ndc^{2-} formed in situ, followed by air oxidation of Mn under the prevailing basic conditions. The reaction is summarized in eq 1.

$$13Mn^{2+} + 10H_2O + 6ndc^{2-} + 2O_2 \rightarrow [Mn_{13}O_8(OH)_6(ndc)_6] + 14H^+ \quad (1)$$

The many oxide and OH^- bridges in **1** are thus concluded to arise from a combination of water in the solvent and the O_2 involved in the reaction. It is thus reasonable that the corresponding reaction in an MeCN/EtOH solvent mixture gives instead $[Mn_{13}O_8(OEt)_5(OH)(ndc)_6]$ (**2**). Clearly, there is enough water in the employed EtOH and atmosphere to compete sufficiently with EtOH for binding. In contrast, using the procedure to **1** using DMF as the reaction solvent but layering with methanol, the product is the corresponding methoxide complex $[Mn_{13}O_8(OMe)_6(ndc)_6]$ (**4**), as concluded from the elemental analysis, infrared spectrum, and similar magnetic behavior (vide infra). We also found that **2** was obtained, but in lower yields, when the triangular $[Mn_3O(O_2CR)_6(py)_3]^+$ (R = Me, Et, Bu^t) complexes were employed in an MeCN/EtOH medium; however, the benzoate complex gives complex **3**, as described below.

For comparison with complexes **1** and **2**, we attempted to prepare the known complex $[Mn_{13}O_8(OEt)_6(O_2CPh)_{12}]$ (**3**) using the published procedure[15] but were unsuccessful. We therefore developed a new, high yield (~80%) synthesis to this compound, the reaction of $[Mn_3O(O_2CPh)_6(py)_2(H_2O)]$ with NEt_3 in MeCN/EtOH. The same product was also obtained from only EtOH solution, but in much lower yield. The Mn_3 reagent is mixed valence ($2Mn^{III}$, Mn^{II}) with an average oxidation state of +2.67, almost identical to that in **3** (+2.62), and EtOH can provide reducing equivalents; this likely contributes to the high yield. The formation of **3** is summarized in eq 2.

$$13[Mn_3O(O_2CPh)_6(py)_2(H_2O)] + 18EtOH + 2e^- \rightarrow 3[Mn_{13}O_8(OEt)_6(O_2CPh)_{12}] + 26pyH^+ + 28PhCO_2^- + 14PhCO_2H + 2H_2O \quad (2)$$

Description of Structures. The structure of complex **1** and a stereopair are presented in Figure 1, and the fully labeled core is shown in Figure 2. Selected interatomic distances are listed in Table 2. Complex **1** crystallizes in the triclinic space group $P\bar{1}$ with the Mn_{13} molecule lying on an inversion center; for the sake of brevity, reference to specific atoms in the following discussion includes their symmetry-related partners. There is a $[Mn_{13}O_8(OH)_6]^{12+}$ core consisting of one Mn^{IV}, six Mn^{III}, and six Mn^{II} atoms bridged by six μ_5-O^{2-}, two μ_3-O^{2-}, and six μ_3-OH^- ions; additional bridging and peripheral ligation is provided by six tetradentate ndc^{2-} groups. All Mn atoms are six-coordinate with near-octahedral geometry, and their oxidation states were established by charge considerations, bond valence sum (BVS) calculations (Table 3), and the clear Jahn−Teller (JT) distortions (axial elongation) at the Mn^{III} atoms (Mn1, Mn2, Mn5), with the JT elongated Mn^{III}−O bonds being at least 0.1−0.2 Å longer than the other Mn^{III}−O bonds. As usual, these JT elongation axes are avoiding the Mn−oxide bonds, in this case pointing toward carboxylate O atoms.

The views in Figures 1 and 2 emphasize that the structure can be described as consisting of three layers: there is a central layer comprising a nearly planar ring of six Mn^{II} atoms (Mn3, Mn4, Mn7) with a Mn^{IV} atom (Mn6) at its center. Above and below this Mn_7 layer is an equilateral triangle of three Mn^{III} atoms (Mn1, Mn2, Mn5) capped by a μ_3-O^{2-} ion (O16); these two triangles are staggered in a trigonal antiprismatic fashion. The Mn^{III}_3 triangles are each connected to the central Mn_7 layer by (i) three μ_5-O^{2-} ions (O13, O18, O19), which have square pyramidal geometry and are bound to $Mn^{II}_2Mn^{III}_2Mn^{IV}$ atoms, and (ii) three μ_3-OH^- ions (O14, O15, O17) bound to $Mn^{II}_2Mn^{III}$ atoms; the O^{2-}/OH^- protonation levels were established by O BVS calculations (Table 3). The peripheral ligation about the resulting $[Mn_{13}O_8(OH)_6]^{12+}$ core is provided by six μ_4-ndc^{2-} groups, each of which has one of its carboxylate groups bridging a Mn^{II}_2 pair and the other bridging a Mn^{III}_2 pair. The resulting molecule has virtual S_6 symmetry, with the S_6 axis passing through the midpoints of the Mn^{III}_3 triangles and the central Mn^{IV} atom. A view approximately along the S_6 axis is provided in Figure 3 (top).

The $[Mn_{13}O_{14}]$ core can alternatively be described as consisting of eight face-fused $[Mn_4O_4]$ cubane units with a common vertex at the central Mn^{IV} atom (Mn6). Each cubane shares three of its faces with its neighbors, creating a larger cubane-like unit whose eight vertices are all O atoms; in this description, the Mn atoms each lie at the midpoint of an edge and at the center of the larger cubane. A view emphasizing this cubic description is provided in Figure 3 (bottom).

It is very interesting and instructive to consider just the Mn atom positions and the resulting Mn_{13} topology. Shown in Figure 4 (top) is the Mn_{13} unit from a viewpoint similar to those in Figures 1 and 2, which emphasizes the $Mn_3/Mn_7/Mn_3$ three-layer arrangement. When viewed from the slightly different viewpoint of Figure 4 (middle), the Mn_{13} unit can now be seen to be a fragment of a body-centered cubic lattice: the fragment comprises one complete body-centered cube with four of its faces capped by the central atoms of four adjacent cubic units. Finally, if the central Mn^{IV} atom is ignored, the remaining Mn_{12} unit is a cuboctahedron (Figure 4 (bottom)). The cuboctahedron is one of the Archimedean solids: it is a polyhedron consisting of six square faces and eight triangular faces and possesses (a) twelve identical vertices (i.e., it is vertex transitive), each representing the meeting point of two triangles and two squares, and (b) twenty-four identical edges, each separating a triangle from a square.[16] The Mn_{13} unit can thus be described as a Mn-centered Mn_{12} cuboctahedron.

The structure of the core of **2** is presented in Figure 5. Selected interatomic distances and angles are listed in Table

(15) Sun, Z.; Gantzel, P. K.; Hendrickson, D. N. *Inorg. Chem.* **1996**, *35*, 6640.

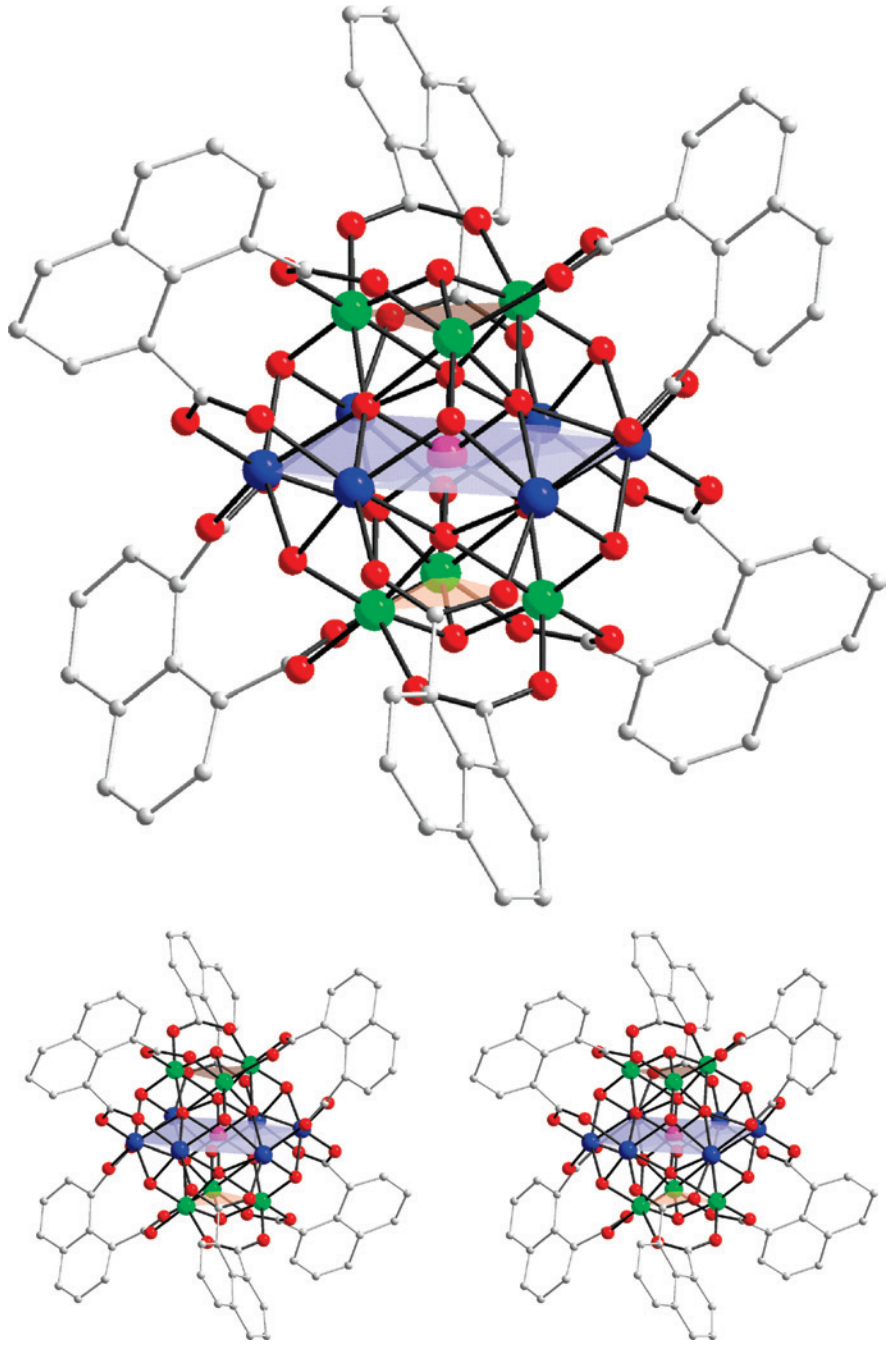

Figure 1. Structure and a stereopair of complex **1**. Hydrogen atoms have been omitted for clarity. Color code: Mn^{II} blue, Mn^{III} green, Mn^{IV} purple, O red, C gray.

4. Complex **2** crystallizes in the triclinic space group $P\bar{1}$ with the Mn_{13} molecule on an inversion center. The complex is again mixed-valence $Mn^{IV}Mn^{III}_6Mn^{II}_6$, as confirmed by BVS calculations (Supporting Information, Table S1), and is structurally almost identical to that of **1** except that there are now five μ_3-EtO^- and one μ_3-OH^- ions in place of the six μ_3-OH^- ions. Peripheral ligation is again provided by six ndc^{2-} groups, and the molecule has virtual S_6 symmetry (ignoring the one OH^- in place of EtO^-). Complex **4** is concluded to be the same as **2** but with MeO^- groups in place of EtO^-.

Complex **3** crystallizes in the monoclinic space group *C2/c*, with the Mn_{13} molecule on an inversion center. It contains benzoate rather than ndc^{2-} groups, and the structure of the complete molecule is shown in Figure 6. The labeled core and a table of selected interatomic distances are provided in Supporting Information, Figure S1 and Table S2, respectively. The complex is $Mn^{IV}Mn^{III}_6Mn^{II}_6$ (Supporting Information, Table S1) and structurally similar to **1** and **2**; its core similar to that in **2**, with six μ_5-O^{2-}, two μ_3-O^{2-}, and six μ_3-EtO^- ions, but it differs markedly from both **1** and **2** in possessing peripheral ligation by twelve benzoate groups, six of them bridging Mn^{II}_2 pairs and six bridging Mn^{III}_2 pairs. The complex again has virtual S_6 symmetry.

A number of mixed-valent $Mn^{II/III/IV}$ clusters have been reported. Our own group has reported Mn_9,[17] Mn_{22},[18] Mn_{25},[19] and Mn_{30}[20] examples, of which the Mn_{25} family are of particular relevance to complexes **1**−**4** in also consisting of

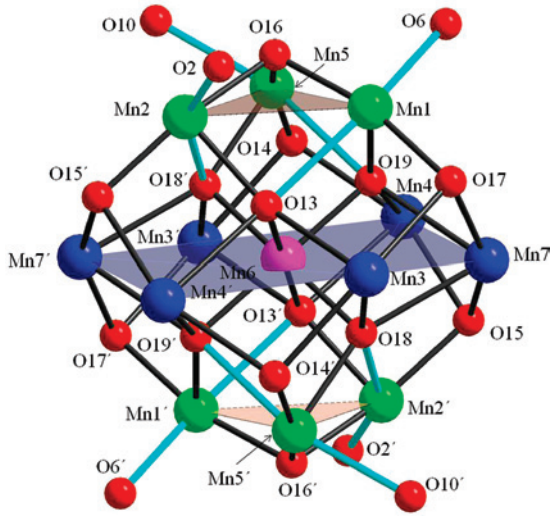

Figure 2. Fully labeled core of complex **1**; primed and unprimed atoms are related by the inversion center. The Mn^{III} Jahn−Teller elongation axes are denoted as sky-blue bonds. Color code: Mn^{II} blue, Mn^{III} green, Mn^{IV} purple, O red.

Table 2. Selected Core Interatomic Distances (Å) for Complex **1**[a]

Mn1···Mn2	2.948(2)	Mn2···Mn6	3.010(1)
Mn1···Mn3	3.173(2)	Mn2···Mn7	3.187(1)
Mn1···Mn5	2.949(2)	Mn3···Mn6	3.218(1)
Mn1···Mn6	3.015(1)	Mn4···Mn7	3.219(2)
Mn2···Mn4	3.205(2)	Mn5···Mn6	3.026(1)
Mn2···Mn5	2.941(2)	Mn4−O15	2.143(5)
Mn1−O16	1.860(5)	Mn4−O19	2.315(5)
Mn1−O17	1.912(5)	Mn4−O14	2.188(5)
Mn1−O19′	1.950(5)	Mn5−O16′	1.866(5)
Mn1−O13	2.330(4)	Mn5−O14	1.921(5)
Mn2−O13	1.960(5)	Mn5−O18	1.954(4)
Mn2−O16	1.890(5)	Mn5−O19	2.353(5)
Mn2−O15	1.921(4)	Mn6−O13	1.878(5)
Mn2−O18′	2.339(5)	Mn6−O18	1.882(5)
Mn3−O18	2.318(5)	Mn6−O19	1.894(4)
Mn3−O12	2.126(6)	Mn7−O17′	2.163(5)
Mn3−O14	2.179(5)	Mn7−O15	2.171(5)
Mn3−O17	2.202(5)	Mn7−O19	2.333(5)
Mn3−O13	2.300(5)	Mn7−O18′	2.350(4)
Mn4−O13	2.391(5)		

[a] The values are for molecule A of the three independent molecules in the unit cell; see the Supporting Information for full details.

Table 3. BVS Calculations for the Mn and μ_3-O Atoms of **1**

atom[a]	Mn^{II}	Mn^{III}	Mn^{IV}
Mn1	3.26	2.98	3.13
Mn2	3.10	2.84	2.98
Mn3	1.92	1.77	1.84
Mn4	1.85	1.69	1.78
Mn5	3.20	2.93	3.07
Mn6	4.34	3.97	4.17
Mn7	1.92	1.76	1.85

atom	BVS	assignment[b]
O14	1.17	OH^-
O15	1.21	OH^-
O16	1.96	O^{2-}
O17	1.19	OH^-

[a] The underlined value is the one closest to the charge for which it was calculated. The oxidation state can be taken as the whole number nearest to the underlined value. [b] An O BVS in the ∼1.8−2.0, ∼1.0−1.2, and ∼0.2−0.4 ranges is indicative of non-, single- and double-protonation, respectively.

Mn_x layers. In particular, the central layer in the Mn_{25} complexes consists of a Mn^{IV}-centered Mn^{III}_6 hexagon, structurally similar to the Mn^{IV}-centered Mn^{II}_6 hexagon of

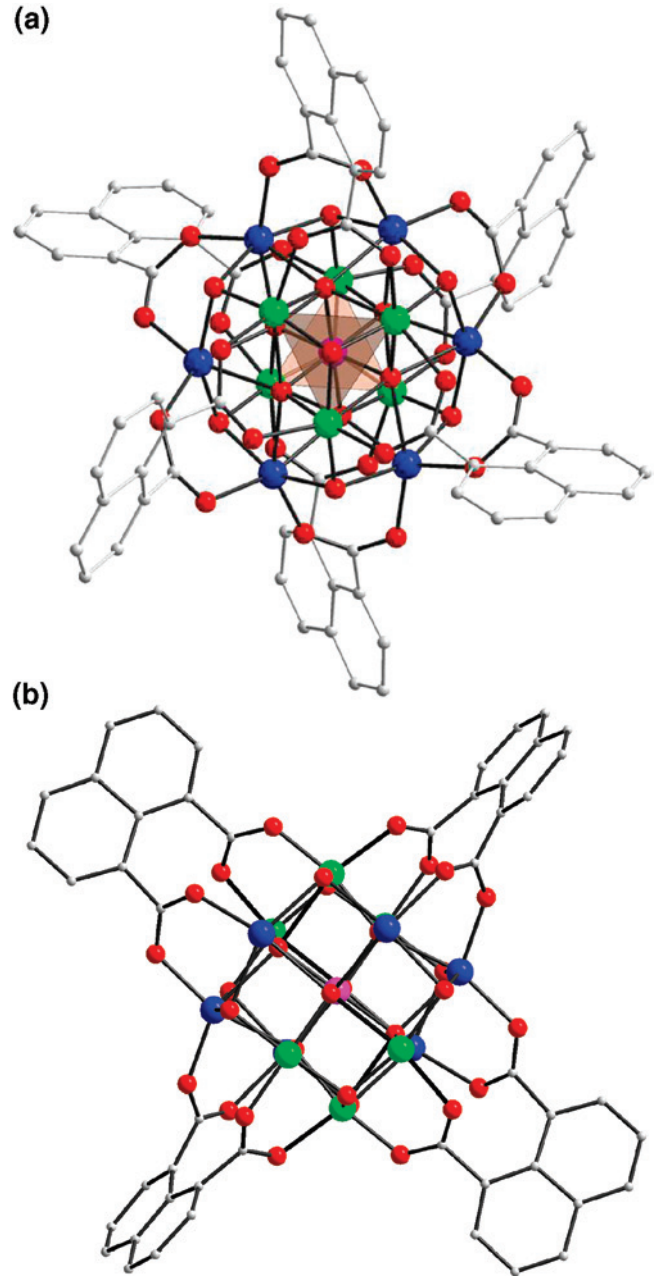

Figure 3. (a) View of complex **1** approximately along the virtual S_6 symmetry axis. (b) View approximately perpendicular to two opposite square faces (with their two bridging ndc^{2-} groups removed for clarity) emphasizing the cubic description of the Mn_{13} core.

1−**4**. Some other multilayered structures include a Mn_{19} family of coordination polymers with a pyramidal structure,[21] a Mn_{13} complex with a dumbbell shape,[22] a Mn_{26} discrete pyramid,[23] a Mn_{18} cluster,[24] a Mn_{10} cage,[25] and a Mn_{19} cluster,[26] as well as the heterometallic $Mn_{10}Th_6$,[27] $Mn_{12}Cu_8$,[28] and $Cu_{17}Mn_{28}$[29] cages, among others. As already mentioned, complex **3** was briefly reported elsewhere,[15] and the Mn_{13} core has also been obtained with ferrocene-1,1′-dicarboxylate[30]a and very recently with another benzoate derivative analogous to **3**.[30]b

Structural Comparison of Complexes 1−3. Since complexes **1**−**3** structurally span differences both in the core (OH^- vs EtO^-) and in the peripheral ligation (ndc^{2-} vs $PhCO_2^-$), and since they display somewhat different mag-

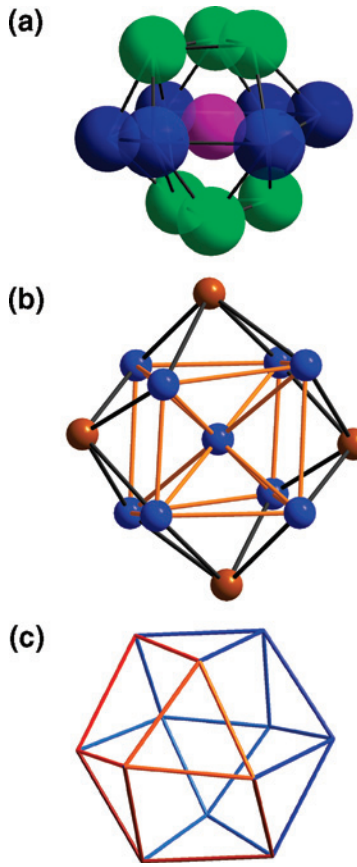

Figure 4. Different views of the Mn_{13} topology: (a) Mn_3, Mn_7, Mn_3 layers, with color code Mn^{IV} purple, Mn^{III} green, Mn^{II} blue; (b) fragment of a body-centered cubic lattice, where the brown atoms are the central atoms of neighboring cubic units; (c) the Mn_{12} cuboctahedron, with the Mn^{IV} at the center omitted.

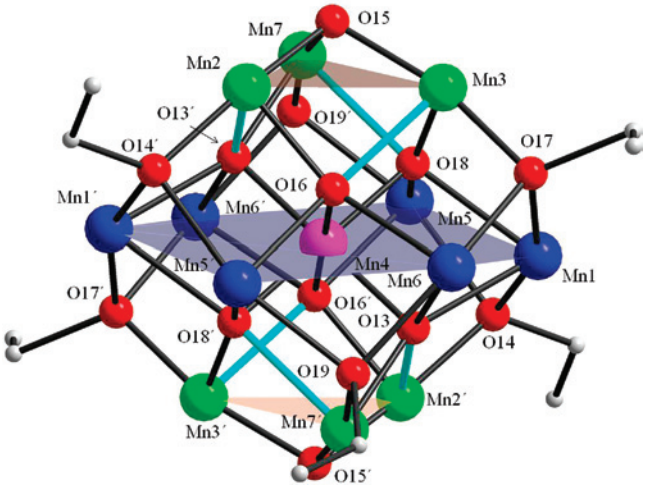

Figure 5. Labeled core of complex **2**; the Mn^{III} JT elongation axes are shown as blue bonds. Color code: Mn^{II} blue, Mn^{III} green, Mn^{IV} purple, O red, C gray.

netic properties (vide infra), it is of interest to assess in more detail any structural differences. Pertinent structural parameters are thus collected in Table 5, and close inspection reveals only a few major differences. The biggest, of course, is the carboxylate C···C separation between two adjacent carboxylate groups. In **1** and **2**, the average separation is only 2.899(42) and 2.909(17) Å, respectively, since the two carboxylate groups are attached to the naphthalene backbone,

Table 4. Selected Core Interatomic Distances (Å) for **2**

Mn1···Mn2	3.174(1)	Mn3···Mn6	3.197(1)
Mn1···Mn4	3.188(1)	Mn4···Mn7	3.054(1)
Mn1···Mn6	3.194(1)	Mn5···Mn6	3.167(1)
Mn2···Mn3	2.977(1)	Mn5···Mn7	3.147(1)
Mn2···Mn4	3.064(1)	Mn6···Mn7	3.139(1)
Mn3···Mn4	3.044(1)	Mn4−O16	1.896(4)
Mn1−O14	2.165(5)	Mn4−O13	1.896(4)
Mn1−O17′	2.182(4)	Mn5−O19	2.168(5)
Mn1−O18′	2.272(5)	Mn5−O14	2.235(4)
Mn1−O13	2.291(4)	Mn5−O16	2.285(4)
Mn2−O15	1.921(5)	Mn5−O18′	2.329(4)
Mn2−O14	1.960(4)	Mn6−O19	2.139(5)
Mn2−O13	1.992(4)	Mn6−O17	2.182(5)
Mn2−O16	2.358(4)	Mn6−O13′	2.262(4)
Mn1−O15	1.891(4)	Mn6−O16	2.340(4)
Mn1−O17	1.915(4)	Mn7−O19	1.898(4)
Mn1−O10′	1.956(4)	Mn7−O15′	1.941(4)
Mn1−O16	1.961(4)	Mn7−O18′	1.994(5)
Mn1−O18	2.357(4)	Mn7−O13′	2.373(4)
Mn4−O18′	1.887(4)		

and these are much shorter than the 3.434(43) Å between two separate benzoate groups in **3**. It is thus logical to assume that this would cause some structural perturbation of the core, but in fact, it does not appear to have a significant effect on the metric parameters within the $[Mn_{13}O_{14}]$ core; those for **3** are almost all within the ranges for either **1** or **2**, or both. In approximately half the entries in Table 5, there are no differences between the three complexes. Among the remainder, it is interesting to note that for some parameters (Mn^{III}···Mn^{III} and Mn^{II}···Mn^{III} distances, and Mn^{III}−μ_3-O^{2-}−Mn^{III} angles), the values for **1** are closer to those for **3** than for **2**. This suggests that, for many of the metric parameters, changes caused by the HO^--to-EtO^- substitution (**1** to **2**) are essentially equal and opposite to those caused by the ndc^{2-}-to-$PhCO_2^-$ substitution (**2** to **3**), resulting in

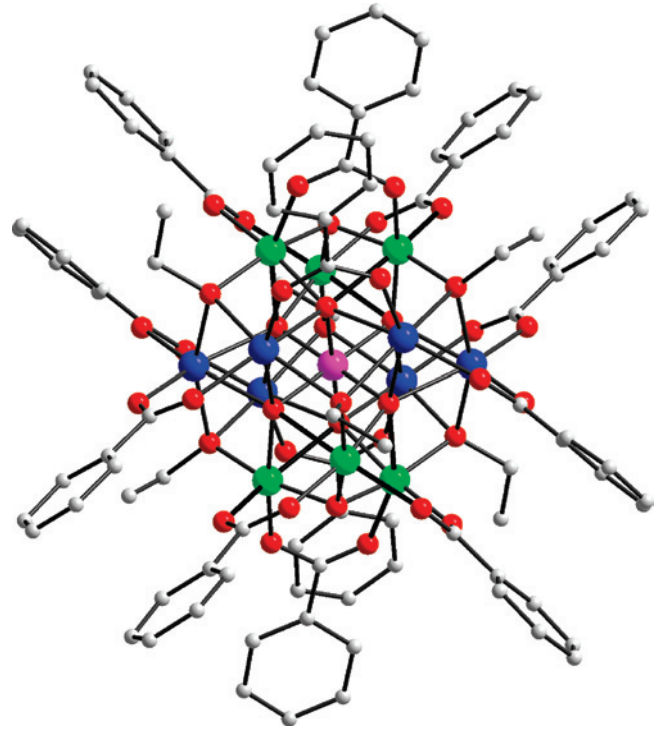

Figure 6. Complete molecule of complex **3**; the Mn^{III} JT elongation axes are shown as thicker black bonds. See Supporting Information for the labeled core. Mn^{II} blue, Mn^{III} green, Mn^{IV} purple, O red, C gray.

Table 5. Structural Comparison between Complexes **1**, **2**, and **3**

parameter[a]	**1**	2	3
C···C (Å)	2.899(42)	2.909(17)	3.434(43)
Mn^{III}···Mn^{III}	2.945(4)	2.987(10)	2.952(3)
Mn^{II}···Mn^{III}	3.186(13)	3.177(38)	3.202(43)
Mn^{II}···Mn^{IV}	3.239(21)	3.195(7)	3.206(8)
Mn^{II}···Mn^{II}	3.250(31)	3.208(41)	3.207(20)
Mn^{III}···Mn^{IV}	3.018(8)	3.054(10)	3.061(80
Mn^{III}−μ_5-O^{2-}−Mn^{III}	86.17(18)	86.43(19)	84.35(35)
Mn^{III}−μ_3-O^{2-}−Mn^{III}	103.85(75)	102.25(45)	104.20(40)
Mn^{II}−O^{2-}−Mn^{IV}	99.93(1.08)	98.54(1.30)	98.85(2.75)
Mn^{III}−O^{2-}−Mn^{IV}	97.16(6.94)	97.42(6.78)	97.40(7.80)
Mn^{II}−O^{2-}-Mn^{II}	88.18(53)	88.15(1.70)	88.41(50)
trans-Mn^{II}−μ_5-O^{2-}−Mn^{III}	162.15(7.65)	162.60(7.90)	161.85(6.55)
cis-Mn^{II}−μ_5-O^{2-}−Mn^{III}	90.66(5.03)	90.41(5.20)	91.55(6.65)
Mn^{II}−RO^{-}−Mn^{III}	102.30(1.60)	101.11(1.26)	100.80(1.60)
Mn^{II}−RO^{-}−Mn^{II}	96.49(2)	94.66(54)	92.30(30)
O^{2-} to Mn_3^{III} plane	0.782	0.837	0.769
Mn^{IV} to Mn_3^{III} plane	2.492	2.520	2.543

[a] Average values, in Å and deg; the range in the values is indicated in parentheses.

some parameters for **1** being the same as those for **3**. In other cases, the values for **2** are closest to those for **3** (e.g., Mn^{II}···Mn^{II}, Mn^{II}···Mn^{IV}, and Mn^{III}···Mn^{IV} distances, Mn^{II}−O^{2-}−Mn^{IV} angles) showing the values are dominated by the EtO^- versus HO^- difference.

With respect to the magnetic properties to be discussed below, a probably significant difference within Table 5 is found in the Mn^{II}−RO^-−Mn^{II} angles, where R = H (**1**) or Et (**2**, **3**). In this case, the values for the latter two are both smaller than that of **1**. This is likely a contributory factor in the observed differences in magnetic properties to be discussed below, because it is well-known that even very small changes in the angles at monatomic bridges between two metal atoms can have a significant effect on the magnitude of the resulting superexchange interaction;[31] this was first demonstrated in the classic work on bis-hydroxo-bridged Cu^{II} dimers.[32]

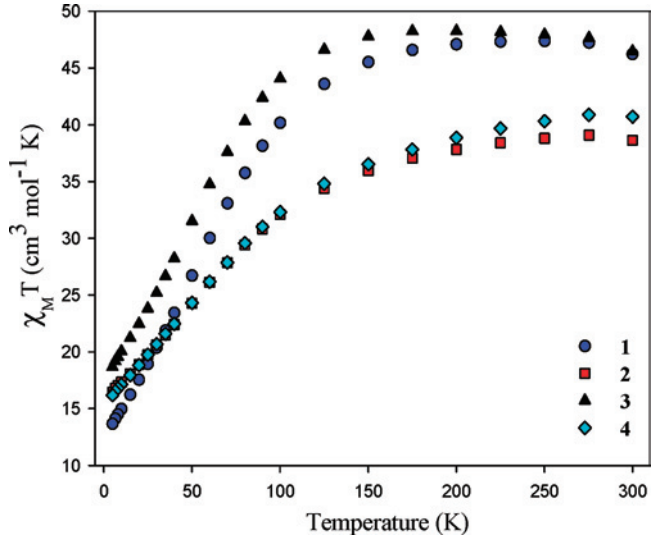

Figure 7. $\chi_M T$ vs T plots for complexes **1**−**4** in the temperature range 5.0−300 K in a 0.1 T, applied dc field.

DC Magnetic Susceptibility Studies on Complexes 1−4. Solid-state, variable-temperature dc magnetic susceptibility (χ_M) data were collected on vacuum-dried microcrystalline samples of complexes **1**−**4**, suspended in eicosane to prevent torquing, in the 5.0−300 K temperature range in a 0.1 T (1000 Oe) magnetic field. The obtained data are plotted as $\chi_M T$ versus T in Figure 7, and it can be seen that the overall profiles are very similar for the four complexes, $\chi_M T$ steadily decreasing with decreasing temperature and thus suggesting dominant antiferromagnetic interactions within the molecules. The plots for **1** and **3** are similar, which is consistent with the two complexes having very similar core metric parameters, as described above. Complexes **2** and **4** exhibit almost identical $\chi_M T$ versus T profiles, and this is reasonable since the two compounds differ only in the EtO^- versus MeO^- difference. We had not pursued the crystal structure of **4** because we did not anticipate that the EtO^- versus MeO^- difference would cause any significant structural difference between the two compounds, and the very similar magnetic properties support this assertion.

The 5.0 K data suggest that the complexes all possess ground states with significant S values. This would not be unexpected for such a complicated Mn_{13} topology with multiple inequivalent exchange parameters, most of which, if not all, being almost certainly antiferromagnetic. This is because of the spin frustration effects expected within the many Mn_3 triangular subunits of the Mn_{13} structure. We define spin frustration here in its more general form as

(16) Keppert, D. L. *Inorganic Stereochemistry*; Springer-Verlag, Berlin, 1982.
(17) Brechin, E. K.; Soler, M.; Christou, G.; Davidson, J.; Hendrickson, D. N.; Parsons, S.; Wernsdorfer, W. *Polyhedron* **2003**, *22*, 1771.
(18) Murugesu, M.; Raftery, J.; Wernsdorfer, W.; Christou, G.; Brechin, E. K. *Inorg. Chem.* **2004**, *43* (14), 4203.
(19) (a) Murugesu, M.; Habrych, M.; Wernsdorfer, W.; Abboud, K. A.; Christou, G. *J. Am. Chem. Soc.* **2004**, *126*, 4766. (b) Stamatatos, T. C.; Abboud, K. A.; Wernsdorfer, W.; Christou, G. *Angew. Chem., Int. Ed.* **2007**, *46*, 884.
(20) (a) Soler, M.; Wernsdorfer, W.; Folting, K.; Pink, M.; Christou, G. *J. Am. Chem. Soc.* **2004**, *126*, 2156–2165. (b) Soler, M.; Rumberger, E.; Folting, K.; Hendrickson, D. N.; Christou, G. *Polyhedron* **2001**, *20*, 1365.
(21) Moushi, E. E.; Stamatatos, T. C.; Wernsdorfer, W.; Nastopoulos, V.; Christou, G.; Tasiopoulos, A. J. *Angew. Chem., Int. Ed.* **2006**, *45*, 7722.
(22) Shanmugam, M.; Chastanet, G.; Mallah, T.; Sessoli, R.; Teat, S. J.; Timco, G. A.; Winpenny, R. E. P. *Chem.—Eur.J.* **2006**, *12*, 8777.
(23) (a) Zaleski, C. M.; Depperman, E. C.; Dendrinou-Samara, C.; Alexiou, M.; Kampf, J. W.; Kessissoglou, D. P.; Kirk, M. L.; Pecoraro, V. L. *J. Am. Chem. Soc.* **2005**, *127*, 12862. (b) Dendrinou-Samara, Alexiou, M.; Zaleski, C. M.; Kampf, J. W.; Kirk, M. L.; Kessissoglou, D. P.; Pecoraro, V. L. *Angew. Chem., Int. Ed.* **2003**, *42*, 3763.
(24) Brechin, E. K.; Clegg, W.; Murrie, M.; Parsons, S.; Teat, S. J.; Winpenny, R. E. P. *J. Am. Chem. Soc.* **1998**, *120*, 7365.
(25) Goldberg, D. P.; Caneschi, A.; Lippard, S. J. *J. Am. Chem. Soc.* **1993**, *115*, 9299.
(26) Ako, A. M.; Hewitt, I. J.; Mereacre, V.; Clerac, R.; Wernsdorfer, W.; Anson, C. E.; Powell, A. K. *Angew.Chem., Int.Ed.* **2006**, *45*, 4926.
(27) (a) Mishra, A.; Abboud, K. A.; Christou, G. *Inorg. Chem.* **2006**, *45*, 2364. (b) Mishra, A.; Tasiopoulos, A. J.; Wernsdorfer, W.; Abboud, K. A.; Christou, G. *Inorg. Chem.* **2007**, *46*, 3105.
(28) Yamashita, S.; Shiga, T.; Kurashina, M.; Nihei, M.; Nojiri, H.; Sawa, H.; Kakiuchi, T.; Oshio, H. *Inorg. Chem.* **2007**, *46*, 3810.
(29) Wang, W. G.; Zhou, A.-J.; Zhang, W.-X.; Tong, M.-L.; Chen, X.-M.; Nakano, M.; Beedle, C. C.; Hendrickson, D. N. *J. Am. Chem. Soc.* **2007**, *129*, 1014.
(30) (a) Kondo, M.; Shinagawa, R.; Miyazawa, M.; Kabir, M. K.; Irie, Y.; Horiba, T.; Naito, T.; Maeda, K.; Utsuno, S.; Uchida, F. *Dalton Trans.* **2003**, 515. (b) Ferguson, A.; Thomson, K.; Parkin, A.; Cooper, P.; Milios, C. J.; Brechin, E. K.; Murrie, M. *Dalton Trans.* **2007**, 728.
(31) Kahn, O. *Molecular Magnetism*; VCH: New York, 1993.
(32) Crawford, W. H.; Richardson, H. W.; Wasson, J. R.; Hodgson, D. J.; Hartfield, W. E. *Inorg. Chem.* **1976**, *15*, 2107.

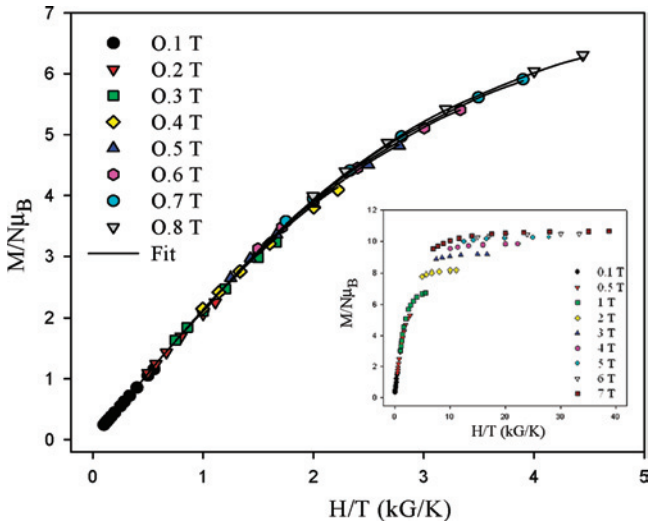

Figure 8. Plot of the reduced magnetization, $M/N\mu_B$, vs H/T for complex **1** in the 0.1−0.8 T field range. The solid lines are the fit with negative D; see the text for the fit parameters. The inset displays the plot of the reduced magnetization in the field range 0.1−7 T.

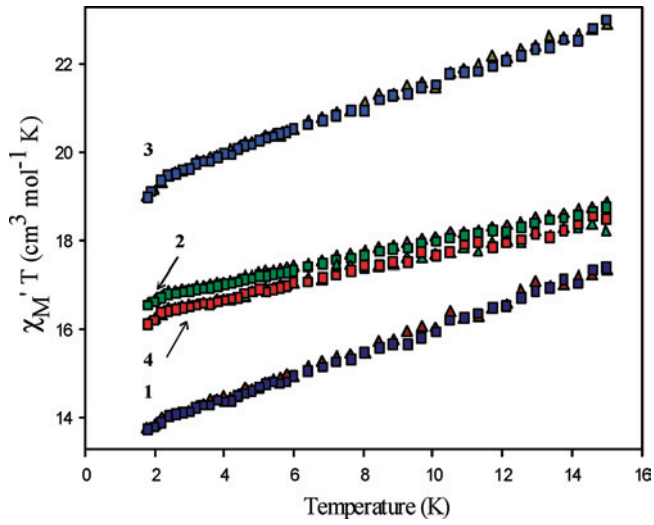

Figure 9. Plot of the in-phase (χ_M') ac magnetic susceptibility as $\chi_M'T$ vs T in a 3.5 Oe field oscillating at 250 (▲) and 1000 (□) Hz for complexes **1**−**4**.

competing exchange interactions of comparable magnitude that prevent (frustrate) the preferred pairwise antiparallel spin alignments that would give small (0 or 1/2) ground states.

To determine the ground states of complexes **1**−**4**, magnetization (M) data were collected in the magnetic field and temperature ranges of 0.1−7 T and 1.8−10 K (Figure 8, inset). We attempted to fit the resulting data using the program MAGNET,[10] which assumes that only the ground-state is populated at these temperatures, includes axial zero-field splitting (ZFS) and the Zeeman interaction, and incorporates a full powder average; the corresponding spin Hamiltonian is given by eq 3.

$$\mathscr{H} = D\hat{S}_z^2 + g\mu_B\mu_0\hat{S}H \qquad (3)$$

However, we could not get an acceptable fit. In our experience, this is the case when there are low-lying excited states that are consequently populated even at these relatively low temperatures, and/or excited states that are more separated from the ground state but have S values greater than that of the ground state and thus their larger M_S levels rapidly decrease in energy because of the applied magnetic field and approach (or even cross) those of the ground state. Such situations are expected for **1**−**4** because of their high content of Mn^{II} atoms, which give very weak and usually antiferromagnetic exchange interactions, and thus low-lying excited states with larger S values.

The above complications can sometimes be avoided by using only data collected at the lowest fields.[19,33] In the present case, a satisfactory fit was obtained for complex **1** using only data collected in the 0.1−0.8 T field range (Figure 8) with fit parameters $S = 9/2$, $g = 2.00(1)$, and $D = -0.14(5)$ cm^{-1}. The narrow range of field data employed will result in a greater-than-usual uncertainty in the obtained D value, which we estimate as indicated but could be even larger. As is usually the case in fitting powder magnetization data, a comparable fit was also obtained with a positive D value, namely, $S = 9/2$, $g = 2.00(1)$, and $D = +0.22(5)$ cm^{-1}. A D versus g root-mean-square error surface (Supporting Information, Figure S2), which plots the relative difference between the experimental $M/N\mu_B$ data and those calculated for various combinations of D and g, indicates that the two fits are of comparable quality and support the significant uncertainties quoted for the fit parameters. Thus, although D values for Mn^{III}-containing Mn_x clusters are almost always negative, this could not be concluded in the present case for **1**. This point was probed further in the EPR studies (vide infra).

For complexes **2**−**4**, we were not satisfied with the quality of the fits even when using data collected at only the lower fields, and we will not discuss them further. In any case, we resorted to the use of more reliable methods employing ac magnetic susceptibility measurements,[34] which do not employ a dc field, to identify the ground spins of **2**−**4**, and also to test our initial conclusion of an $S = 9/2$ ground state for **1**.

AC Magnetic Susceptibility Studies on Complexes 1−4. Alternating-current magnetic susceptibility studies were performed on vacuum-dried microcrystalline samples of **1**−**4** in the temperature range 1.8−15 K in a zero dc field and a 3.5 Oe ac field oscillating at frequencies between 250−1000 Hz. The resulting data are plotted as $\chi_M'T$ versus T in Figure 9, where χ_M' is the in-phase component of the ac susceptibility. For all four complexes, $\chi_M'T$ decreases essentially linearly with decreasing temperature, this downward slope supporting a decreasing population of excited states with a larger S than the ground state, in agreement with the statements above re

(33) (a) Soler, M.; Wernsdorfer, W.; Folting, K.; Pink, M.; Christou, G. *J. Am. Chem. Soc.* **2004**, *126*, 2156. (b) Sanudo, E. C.; Wernsdorfer, W.; Abboud, K. A.; Christou, G. *Inorg. Chem.* **2004**, *43*, 4137. (c) Murugesu, M.; Raftery, J.; Wernsdorfer, W.; Christou, G.; Brechin, E. K. *Inorg. Chem.* **2004**, *43*, 4203.

(34) (a) Brechin, E. K.; Boskovic, C.; Wernsdorfer, W.; Yoo, J.; Yamaguchi, A.; Sanado, E. C.; Concolino, T. R.; Rheingold, A. L.; Ishimoto, H.; Hendrickson, D. N.; Christou, G. *J. Am. Chem. Soc.* **2002**, *124*, 9710. (b) Sanudo, E. C.; Wernsdorfer, W.; Abboud, K. A.; Christou, G. *Inorg. Chem.* **2004**, *43*, 4137. (c) Soler, M.; Rumberger, E.; Folting, K.; Hendrickson, D. N.; Christou, G. *Polyhedron* **2001**, *20*, 1365.

the dc magnetization fitting problems. A linear extrapolation of the data for **1** to 0 K, where only the ground state will be populated, gives $\chi_M'T$ of ~13 cm^3 K mol^{-1}, indicating an $S = 9/2$ ground state (expected spin-only ($g = 2.0$) values for $S = 7/2$, 9/2, and 11/2 are 7.88, 12.4, and 17.88 cm^3 K mol^{-1}). This is in satisfying agreement with the dc magnetization fit in Figure 8. For **2** and **4**, the plots are almost superimposed and the $\chi_M'T$ values are significantly higher, extrapolating to values in the 16.0−16.5 cm^3 K mol^{-1} range at 0 K, consistent with an $S = 11/2$ ground state for these complexes. Again, their anticipated similarity in structure is supported by their almost identical magnetic properties. For **3**, the $\chi_M'T$ versus T plot is noticeably higher than those for the other complexes and appears to be heading for a value in the 18.5−19.0 cm^3 K mol^{-1} range. Again, this is suggestive of an $S = 11/2$ ground state, since the expected spin-only value for an $S = 13/2$ state is much higher at 24.38 cm^3 K mol^{-1}. The slightly high value for **3** is likely caused by one or more particularly low-lying excited states whose depopulation does not become evident in the $\chi_M'T$ versus T plot until the very lowest temperatures, below the 1.8 K operating limit of our SQUID magnetometer. The same may apply for the slightly high value for **1**. Note that deviations of g from 2.0 should be below not above this value for Mn.

It is interesting that complexes **1** and **3** have the overall more similar $\chi_M T$ versus T behavior up to 300 K (Figure 7) but that **2**, **3**, and **4** are the more similar in ground state (Figure 9). The former observation is consistent with the many structural similarities between **1** and **3** seen in Table 5, even though they differ in both the EtO^- versus HO^- and benzoate versus ndc^{2-} identities, whereas the difference in ground state is perhaps caused by the significantly different $Mn^{II}Mn^{II}$ exchange interactions via the $Mn^{II}-RO^--Mn^{II}$ (R = H, Et) superexchange pathways. These are likely the weakest interactions in the molecule; their impact thus becomes evident only at the lowest temperatures. Given the significant difference in these angles, it seems reasonable that it could cause a flip in the relative energies of some of the closely separated, lowest-lying spin states, causing a change in the ground state. In contrast, the MeO^- versus EtO^- difference between **2** and **4** has essentially no impact on the magnetic properties. Finally, none of the compounds exhibited a frequency-dependent drop in the $\chi_M'T$ versus T plot at the lowest temperatures or an out-of-phase χ_M'' signal, and we conclude that they are not SMMs. The tiny dips in the plots of Figure 9 at ~2 K are not frequency-dependent and are likely caused by very weak intermolecular interactions.

Single-Crystal, High Frequency EPR (HFEPR) Spectroscopy. HFEPR spectra on a single crystal of representative complex **1**·*x*DMF were obtained at 51.8 GHz to probe the magnitude and sign of the D value. The spectra revealed a single broad peak throughout the 2.5−20 K range, with no discernible fine structure (Figure 10). The position of this peak (1.86 T) corresponds very precisely to the isotropic $g = 2.00(1)$ value. A very faint peak can be seen at ~0.93 T, but this corresponds simply to a double quantum ($g = 4.00$) transition, that is, this peak is observed at exactly half the field of the main peak. Measurements were also carried out at several higher frequencies (Figure 11), and these gave the same conclusions, that is, the peak positions lie on two straight lines corresponding to $g = 2.000(5)$ and 3.98(3). We also carried out angle-dependent studies at 10 K (Figure 10a), and these revealed no detectable variation in the position of the 1.86 T peak for 180° of rotation. These combined data suggest that complex **1**·*x*DMF possesses little or no magnetic anisotropy.

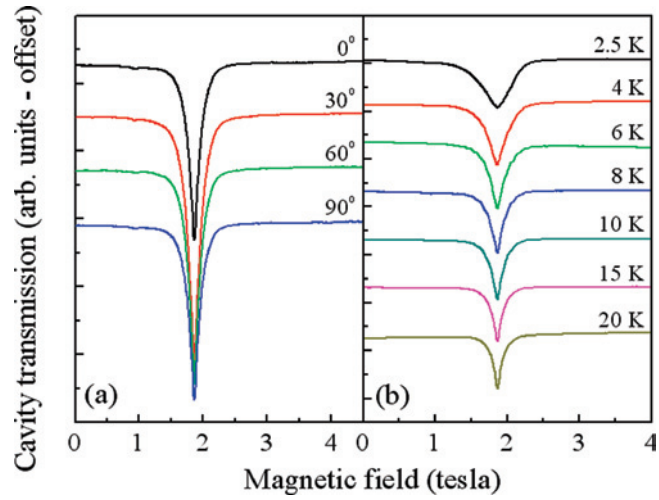

Figure 10. (a) Angle-dependent EPR spectra obtained at 51.8 GHz and 10 K. (b) Temperature dependence of the EPR spectrum at 51.8 GHz.

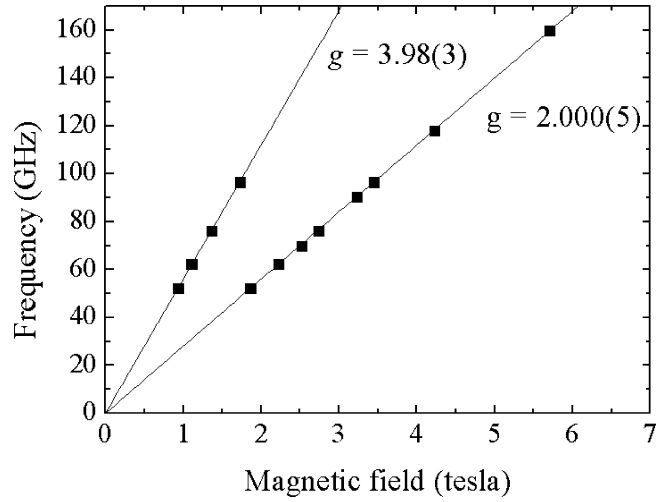

Figure 11. Frequency dependence of the EPR spectrum. The solids lines are the fits and the obtained g values.

The only slight hint that magnetic anisotropy could be present for **1**·*x*DMF was obtained upon cooling the sample to 2.5 K (Figure 10b), whereupon the main EPR peak became broader and displayed slight asymmetry. This behavior may be indicative of the appearance of unresolved fine-structure caused by weak ZFS.[35] However, given that it is not possible to resolve any fine-structure splitting, we are unable to make any quantitative statements about either the magnitude of the ground state S value or the axial ZFS parameter (D) for **1**·*x*DMF on the basis of these EPR measurements.

Overall, the EPR studies suggest that complex **1** is essentially isotropic, that is, $D \approx 0$. Indeed, on the basis of

(35) Murugesu, M.; Takahashi, S.; Wilson, A.; Abboud, K. A.; Wernsdorfer, W.; Hill, S.; Christou, G. *Inorg. Chem.* **2008,** *47*, 9459.

the EPR line width, it is unlikely that the magnitude of $|D|$ could be greater than 0.05 cm^{-1}. The latter is somewhat smaller than that obtained from the dc magnetization fit, which was $D = -0.14(5)$ cm^{-1} (assuming the negative value). Of course, the inversion symmetry of the Mn_{13} molecules, and the arrangement of the Mn^{III} JT axes (Figure 2) suggest that D should indeed be essentially zero. We note three pertinent points: (i) the HFEPR studies were on a single crystal of **1**·*x*DMF ($x \approx 19$) kept wet with mother liquor, whereas the dc magnetization data were collected on dried samples analyzing as **1**·8DMF·H_2O. It is quite possible that solvent loss could cause some crystal lattice collapse and resulting small perturbations of the Mn_{13} molecules affecting the D value;[36] (ii) the low-lying excited states may be particularly problematic in this case, and the obtained D value thus artificially high; and (iii) bulk magnetization studies are not the most accurate way to determine D, and although there is usually better agreement between magnetization fits and EPR data, it is possible in this case that the former are particularly unreliable. Points (ii) and (iii) are likely cause-and-effect, and in fact, it is very possible that all three points (i−iii) are contributing to the difference in D from the magnetization and HFEPR studies in the present work. In any event, it is clear that the value obtained from the EPR data is a much more reliable measure of the true D value of the compound.

Conclusions

The initial use of the ndc^{2-} dicarboxylate group in Mn chemistry has led to three mixed-valent Mn_{13} clusters containing three different oxidation states of this metal and differing only in the HO^- versus MeO^- versus EtO^- identity of some of the bridging ligands. In addition, a rational and convenient synthesis has been developed for the known benzoate version. This Mn_{13} family has a very interesting core structure, with the Mn_{13} topology comprising a Mn-centered cuboctahedron, or alternatively a fragment of a body-centered cubic lattice. Comparison of the structural parameters of **1**−**3** reveal that the inflexible ndc^{2-} group imposes only minor structural changes on the cores of **1** and **2** compared with the monocarboxylate benzoate ligation in **3**. Nevertheless, complex **1** has a lower ground-state spin of $S = 9/2$, whereas the others have $S = 11/2$ ground states. As expected from the distribution and orientation of the Mn^{III} JT distortion axes, the complexes have little magnetoanisotropy, as reflected in the axial ZFS parameter, D. HFEPR studies on single crystals of the representative complex **1**·*x*DMF revealed it to be essentially isotropic, a relatively rare situation, in fact, for such a high nuclearity cluster. As a result, there was no possibility of these compounds functioning as SMMs. Nevertheless, the unusual η^1:η^1:η^1:η^1:μ_4 coordination mode adopted by the ndc^{2-} group suggests that it may yet prove a route to many other high nuclearity products, both homo- and heterometallic, and some of these could well be new members of the SMM family. Further studies are thus in progress along these lines.

Acknowledgment. This work was supported by NSF (CHE-0414555).

Supporting Information Available: X-ray crystallographic data in CIF format for complexes **1**−**3**, two-dimensional contour plot of the error surface for the magnetization fit for **1,** BVS calculations for **2** and **3**, and selected interatomic distances for **3**. This material is available free of charge via the Internet at http://pubs.acs.org.

IC801484G

(36) Karadas, F.; Schelter, E. J.; Shatruk, M.; Prosvirin, A. V.; Bacsa, J.; Smirnov, D.; Ozarowski, A.; Krzystek, J.; Telser, J.; Dunbar, K. R. *Inorg. Chem.* **2008**, *47*, 2074.